Valley dynamics of intravalley and intervalley multiexcitonic states in monolayer WS_2

Jiyong Fu,[1,2,*] Andre Bezerra,[2] and Fanyao Qu[2,†]
[1]*Department of Physics, Qufu Normal University, 273165 Qufu, Shandong, China*
[2]*Instituto de Física, Universidade de Brasília, Brasília-DF 70919-970, Brazil*

(Received 1 October 2017; revised manuscript received 17 December 2017; published 19 March 2018)

We present a comprehensive model comprising of a complete set of rate equations, which account for charge transfer among multiexcitonic channels including excitons, trions, and biexcitons, to investigate valley (locked with spin) dynamics in monolayer WS_2. The steady-state photoluminescence (PL) spectra, underlying the laser power dependence of excitonic populations, are also determined. Our computed PL for all excitonic states agrees with the experimental data of Paradisanos *et al.* [Appl. Phys. Lett. **110**, 193102 (2017)]. We find that the relative weight of PL, stemmed from different excitonic channels, strongly depends on the laser power even under dynamical conditions. Remarkably, the biexciton channel, having the weakest PL intensity at low laser powers, tends to prevail in PL over other excitonic states as the power strengthens. In addition, by accounting for intervalley scatterings, which enable transfer of excitonic states from one valley to the other, we determine the valley polarization, which strongly depends on intervalley scatterings and the exciton generation rates in the two valleys. On the other hand, the valley polarization for all excitonic channels is found almost independent of the laser power, consistent with experimental measurements as well. Finally, the valley dynamics involving both intra- and intervalley trions is discussed. Our model and numerical outcome should be beneficial to experiments especially featuring the interplay of multiexcitonic channels in, e.g., elucidating experimental data, estimating central excitonic quantities including recombination times and transition rates, and in widening possible new experimental scopes.

DOI: 10.1103/PhysRevB.97.115425

I. INTRODUCTION

Monolayer semiconducting transition metal dichalcogenides (TMDCs) denoted by MX_2 (M = Mo, W; S = S, Se, Te) have attracted considerable interest following the discovery of a direct band gap at the two inequivalent K and K' valleys [1–6] and of the coupling of spin and valley degrees of freedom (i.e., spin-valley locking) [7–11] due to the joint effect of lattice inversion asymmetry and spin-orbit interaction. This leads to valley (and spin) selective optical transitions depending on the pumping photon helicity [7,12,13], and further allows for optical generation of valley polarization (optical orientation) [14–16], valley Hall effect [2,9], valley coherence [17–20], and optical manipulation of valley pseudospin [21].

Moreover, large electron and hole effective masses along with reduced dielectric screening in monolayer TMDCs of two-dimensional (2D) characters yield exceptionally strong Coulomb interaction between charged carriers [23,24]. This results in the formation of tightly bound electron-hole pairs, namely excitons (X) [12]. In the presence of residual excess charges, Coulomb interaction could further bind an excess charge to one exciton to form a charged exciton, i.e., trion (negative X^- and positive X^+) [25], with X^- or X^+ depending on doping conditions [26]. In addition, strong Coulomb interaction also favors the Auger-type exciton-exciton annihilation process [27], leading to the formation of biexcitons (molecule-like states consisting of two excitons), which can maintain stable even at extremely low laser power densities (∼0.2 kW cm^{-2}) [28]. The binding energy of these excitonic quasiparticle states in TMDCs is extraordinarily appealing, with several hundred meV for excitons and a range of 30–70 meV for trions and biexcitons [29], allowing them to exist even at room temperature [22], extremely challenging in conventional semiconductors.

The spin-valley locked band structure could not only accommodate bright excitonic states [30,31], but also hold optically inaccessible dark excitonic ones [27,32], of both intravalley (spin forbidden) [33,34] and intervalley (momentum forbidden) types [35]. Bright and dark excitons are split primarily by the spin-orbit splitting of the conduction band, with the lowest-lying excitonic states being optically dark in W-based monolayer TMDCs but optically bright in Mo-based ones [35,36]. The existence of dark excitons has been experimentally identified through time-resolved photoluminescence (PL) spectroscopy [37] and magneto-PL [38,39]. Very recently, the entire dark exciton landscape in TMDCs was revealed via infrared spectroscopy [40,41].

These excitonic quasiparticle states are of crucial importance for exploiting the optical properties of TMDCs [13,42]. For identifying PL emission bands with multiexcitonic channels and investigating the valley (locked with spin) dynamics, there have been extensive studies carried out in experiments through, e.g., time-resolved PL [43,44], ultrafast transient absorption spectroscopy [45], and time-resolved Kerr rotation [46,47]. However, from the theoretical perspective, available models for valley dynamics in TMDCs only accounted for the

*jiyongfu78@gmail.com
†fanyao@unb.br

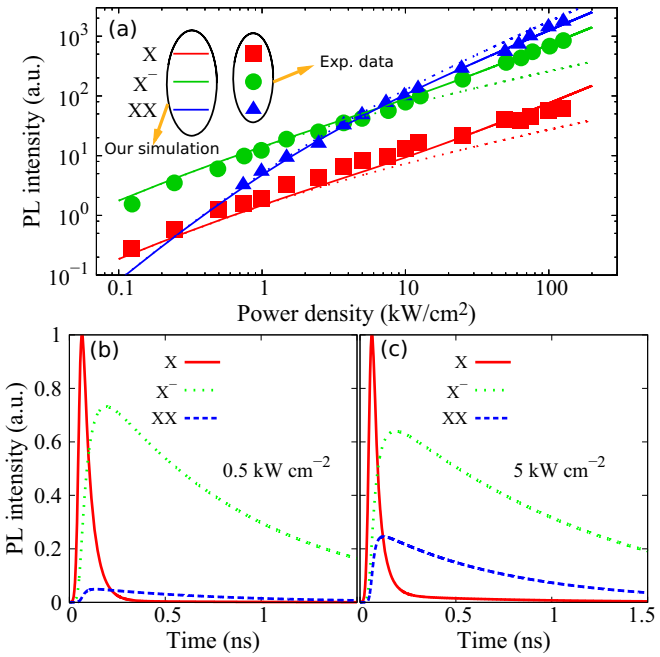

FIG. 1. (a) PL intensity of exciton (X), trion (X^-), and biexction (XX) in monolayer WS_2 as a function of excitation laser power density. The markers refer to the experimental data of Ref. [22] and the curves are obtained from our simulation. The dotted lines indicate the simulated PL intensity for constant exciton-to-biexciton transition rate ($\beta = \beta_0$), i.e., neglecting the power dependence of β, which is inconsistent with the experimental data at high power densities. Time evolution of PL for X, X^-, and XX at a power density of 0.5 (b) and 5 kW cm^{-2} (c). In (b) and (c), the PL intensity is normalized with respect to the corresponding exciton PL peak, and a Gaussian pulse duration of 30 ps is considered.

scattering between two quasiparticles (channels), e.g., X and X^- or X and XX [15,43,44,48], and were mainly restricted within a single *isolated* valley [33,49], and thus is only applicable for some special and even limited circumstances. Thereby, a comprehensive theory to study the valley dynamics of coexisting multiexcitonic states of both intra- and intervalley types, is greatly desired, but is still not available.

Here we mainly focus on bright excitons and develop a comprehensive model composed of a complete set of rate equations, taking into account charge transfer among intra- and intervalley multiexcitonic states. Then we compute with our model the PL intensity, which is proportional to the concentration of optically generated excitonic states, allowing us to determine the valley dynamics and valley polarization. In addition to the dynamical evolution of PL, we also consider its power dependence in steady state. Our computed PL for all excitonic channels in monolayer WS_2 is consistent with experimental data of Ref. [22], Fig. 1(a). We further go beyond and take into account intervalley scatterings and intervalley excitonic states [50–53]. Finally, we discuss the potential effect of dark excitons on valley dynamics.

This paper is organized as follows. In Sec. II we present our model for valley dynamics of bright excitons. We consider three different cases, with (i) multiexcitonic states in a single isolated valley (i.e., no intervalley scattering), (ii) intravalley excitonic states with intervalley scatterings, and (iii) both intra- and intervalley excitonic states, referring to three distinct experimental conditions. In Sec. III we discuss our numerical outcome computed from our model. We summarize our main findings in Sec. IV.

II. MODEL: A COMPLETE SET OF RATE EQUATIONS

The interplay of inversion asymmetry and spin-orbit interaction in monolayer TMDCs leads to valley-contrasting spin splittings (spin-valley locking) *bridged* by time reversal symmetry, for both the valence and conduction bands [9]. The spin splitting of the valence band, arising primarily from the transition metal d orbital, is around hundreds of meV [54], far greater than that of the conduction band ranging from several to tens of meV [55]. As a consequence, optically allowed interband transitions from the two spin states of the valence band are well separated, referring to A and B excitons, respectively. This allows us to develop our theory within only three bands, consisting of one spin branch of the valence band with higher energy and both spin branches of the conduction band (A exciton transition); see the band dispersion around the K (K') valley of monolayer WS_2, Fig. 2.

The spin states of the conduction band could have opposite ordering in energy [55], depending on transition metal atoms, as opposed to that of the valence band. This leads to the lowest energy transition (ground state) being optically bright (same spin, spin allowed) in MoX_2 and optically dark (opposite spin, spin forbidden) in WX_2. Here we restrict our discussions to WS_2, but the study can be straightforwardly extended to Mo-based TMDCs. In addition, to verify our model, we aim to first simulate the experimental data of Ref. [22] obtained at a high temperature of 200 K. Since the lowest energy transition in WS_2 is optically dark, a high temperature could drive dark excitons away from the ground state to become optically bright, thus greatly suppressing the effect of dark excitons on valley dynamics. As a result, in this section we only focus on bright excitonic states in our model, Fig. 2, and more discussions about dark exciton mediated valley dynamics will be given in Sec. III D.

To systematically describe excitonic valley dynamics, we develop our theory in three different cases, referring to three distinct experimental conditions, i.e., (i) multiexcitonic states in a single isolated valley, (ii) intravalley excitonic states with intervalley scatterings, and (iii) both intra- and intervalley excitonic states, as schematically shown in Figs. 2(a)–2(c), respectively.

A. Valley dynamics of muliexcitonic states in a single valley

We start with the simplest case, case I, Fig. 2(a), in which only intravalley excitonic states and intravalley scatterings are involved, i.e., no charge transfer between the K and K' valleys. Since the states of the two valleys are related by time reversal symmetry, we consider in case I the excitonic states only residing in the K valley, implying that the K' valley constantly remains unpopulated. Under these considerations,

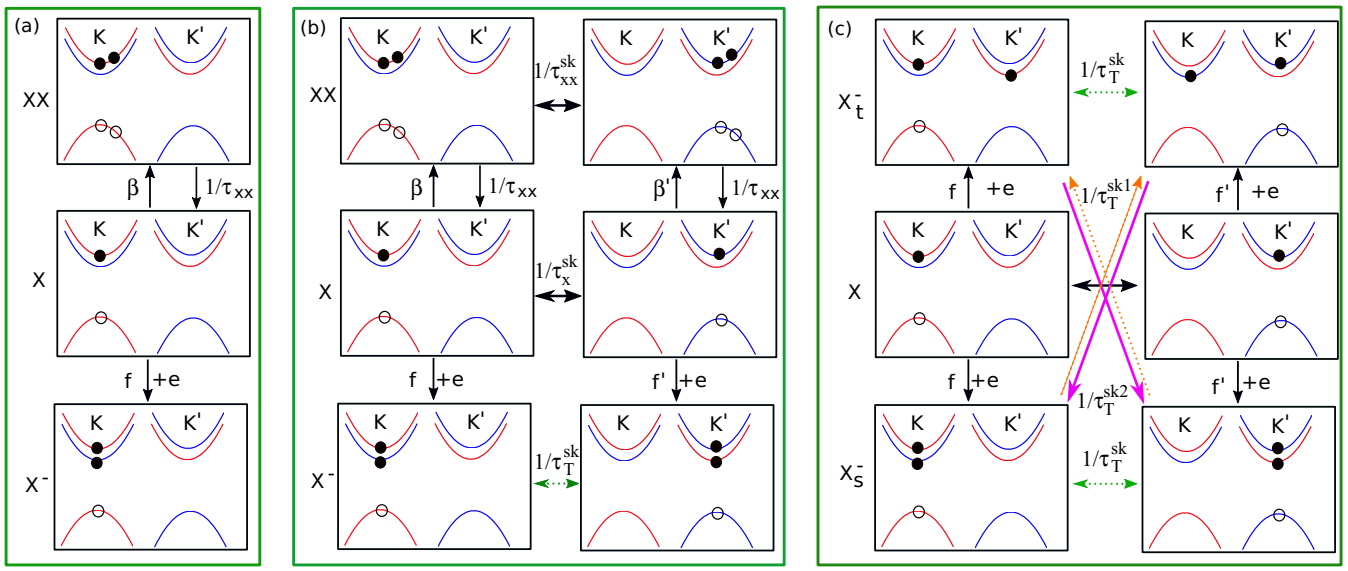

FIG. 2. Schematic of scatterings among different excitonic states in monolayer WS_2, with the red (blue) curves standing for spin-up (spin-down) conduction band and valence band in the K and K' valleys and filled (empty) black circles representing electrons (holes). (a) Intravalley excitonic states (XX, X, X^-) and scatterings in the K valley; (b) intravalley excitonic states (XX, X, X^-) in the K and K' valleys with intra- and intervalley scatterings; (c) intravalley exciton (X), intravalley trion (spin singlet, X_s^-), and intervalley trion (spin triplet, X_t^-) with intra- and intervalley scatterings. In (a) the K' valley is constantly unpopulated and in (b) and (c) both the K and K' valleys are occupied. The transition rates β, β', f, f', $1/\tau_{xx}$, $1/\tau_{xx}^{sk}$, $1/\tau_x^{sk}$, $1/\tau_T^{sk}$, $1/\tau_T^{sk1}$, and $1/\tau_T^{sk2}$ are defined in Eqs. (1)–(3). Dotted arrows (green and orange) indicate that the relevant transition process are relatively slow compared to other processes.

the dynamics of the intravalley X, X^-, and XX is described by

$$\begin{aligned}
\frac{dn_x}{dt} &= g - \frac{n_x}{\tau_x} - f n_x n_e + \frac{n_{xx}}{\tau_{xx}} - 2\beta n_x^2,\\
\frac{dn_T}{dt} &= -\frac{n_T}{\tau_T} + f n_x n_e,\\
\frac{dn_{xx}}{dt} &= -\frac{n_{xx}}{\tau_{xx}} + \beta n_x^2,
\end{aligned} \tag{1}$$

where n_x, n_T, and n_{xx} are excitonic concentrations in the K valley, and τ_x, τ_T, and τ_{xx} are the corresponding recombination times, with the subscript x, T, and xx standing for excitons, trions, and biexcitons, respectively; g denotes the exciton generation rate; β and f [cf. Eq. (1) and Fig. 2(a)] separately represent the exciton-to-biexciton (i.e., exciton-exciton annihilation) and exciton-to-trion (i.e., exciton-electron scattering) transition rates; and n_e is the electron density in an n-type monolayer TMDC.

We emphasize that we take into account in our simulation the laser power dependence of the exciton-to-biexciton transition rate $\beta = \beta_0/(1 + P/P_0)$ [43], with P the laser power. We find this relation is essential in our simulated PL intensity especially at high laser powers, cf. solid and dotted curves in Fig. 1(a), as a result of biexcitons due to its quadratic behavior of increments increasing more dramatically [Eq. (1)] than trions. Although the remaining parameters including those below in Eqs. (2) and (3) may in principle also depend on the laser power, the dependence is assumed relatively weak, and hence they are considered constant. Moreover, we have presumed the decay of a biexciton leads to the generation of one exciton [43], cf. Eq. (1) and Fig. 2(a).

B. Valley dynamics of intravalley excitonic states with intervalley scatterings

Before moving to case II, it is worth pointing out that despite the large separation (comparable to the size of Brillouin zone) between the K and K' valleys, spin-valley locking, and giant valence-band spin-orbit splitting [9], all of which suppress the scatterings [9], experimental measurements have revealed the fast decay of valley polarization [32,56]. This is ascribed to effective intervalley scatterings, induced by atomic defects and/or electron-hole exchange interaction [32,56]. Accordingly, in case II, Fig. 2(b), we extend our theory in the previous scenario by adding the intervalley scatterings, triggering charge transfer from one valley to the other. Then we have in this case a new set of rate equations, which are written as

$$\begin{aligned}
\frac{dn_x}{dt} &= g - \frac{n_x}{\tau_x} - \frac{n_x}{\tau_x^{sk}} + \frac{n'_x}{\tau_x^{sk}} - 2\beta n_x^2 + \frac{n_{xx}}{\tau_{xx}} - f n_x n_e,\\
\frac{dn'_x}{dt} &= g' - \frac{n'_x}{\tau_x} - \frac{n'_x}{\tau_x^{sk}} + \frac{n_x}{\tau_x^{sk}} - 2\beta' {n'_x}^2 + \frac{n'_{xx}}{\tau_{xx}} - f' n'_x n'_e,\\
\frac{dn_{xx}}{dt} &= -\frac{n_{xx}}{\tau_{xx}} + \beta n_x^2 - \frac{n_{xx}}{\tau_{xx}^{sk}} + \frac{n'_{xx}}{\tau_{xx}^{sk}},\\
\frac{dn'_{xx}}{dt} &= -\frac{n'_{xx}}{\tau_{xx}} + \beta' {n'_x}^2 - \frac{n'_{xx}}{\tau_{xx}^{sk}} + \frac{n_{xx}}{\tau_{xx}^{sk}},\\
\frac{dn_T}{dt} &= -\frac{n_T}{\tau_T} + f n_x n_e - \frac{n_T}{\tau_T^{sk}} + \frac{n'_T}{\tau_T^{sk}},\\
\frac{dn'_T}{dt} &= -\frac{n'_T}{\tau_T} + f' n'_x n'_e - \frac{n'_T}{\tau_T^{sk}} + \frac{n_T}{\tau_T^{sk}},
\end{aligned} \tag{2}$$

where all physical quantities (e.g., n_x) in the K valley maintain the same as those defined in Eq. (1), while their counterparts (e.g., n'_x) in the K' valley are labeled by a superscript "$\prime$" for differentiation. The quantities τ_x^{sk}, τ_T^{sk}, and τ_{xx}^{sk}, absent in Eq. (1), represent relevant intervalley scattering times for X, X^-, and XX, respectively, cf. Eq. (2) and Fig. 2(b).

C. Valley dynamics of both intravalley and intervalley excitonic states

With the knowledge of valley dynamics presented in cases I and II, we are ready to explore more complex dynamics, case III, Fig. 2(c), in which the intervalley excitonic states are taken into account. We consider both intravalley trions (spin singlet, X_s^-) and intervalley trions (spin triplet, X_t^-), the formation of which depends on whether or not the *captured* electron resides in the same valley as the exciton it is bound to. For simplifying discussions, here we exclude the biexciton channel. Since we only focus on the bright excitonic states, the intervalley exciton (optically dark) [27] is also precluded as well. Then, the set of rate equations describing charge transfer among X, X_s^-, and X_t^- with both intra- and intervalley scatterings taken into account, are written as

$$
\begin{aligned}
\frac{dn_x}{dt} &= g - \frac{n_x}{\tau_x} - \frac{n_x}{\tau_x^{sk}} + \frac{n'_x}{\tau_x^{sk}} - f n_x n_e - f n_x n'_e,\\
\frac{dn'_x}{dt} &= g' - \frac{n'_x}{\tau_x} - \frac{n'_x}{\tau_x^{sk}} + \frac{n_x}{\tau_x^{sk}} - f' n'_x n'_e - f' n'_x n_e,\\
\frac{dn_{T,t}}{dt} &= -\frac{n_{T,t}}{\tau_{T,t}} + f n_x n'_e - \frac{n_{T,t}}{\tau_T^{sk}} + \frac{n'_{T,t}}{\tau_T^{sk}} - \frac{n_{T,t}}{\tau_T^{sk2}} + \frac{n'_{T,s}}{\tau_T^{sk1}},\\
\frac{dn'_{T,t}}{dt} &= -\frac{n'_{T,t}}{\tau_{T,t}} + f' n'_x n_e - \frac{n'_{T,t}}{\tau_T^{sk}} + \frac{n_{T,t}}{\tau_T^{sk}} - \frac{n'_{T,t}}{\tau_T^{sk2}} + \frac{n_{T,s}}{\tau_T^{sk1}},\\
\frac{dn_{T,s}}{dt} &= -\frac{n_{T,s}}{\tau_{T,s}} + f n_x n_e - \frac{n_{T,s}}{\tau_T^{sk}} + \frac{n'_{T,s}}{\tau_T^{sk}} - \frac{n_{T,s}}{\tau_T^{sk1}} + \frac{n'_{T,t}}{\tau_T^{sk2}},\\
\frac{dn'_{T,s}}{dt} &= -\frac{n'_{T,s}}{\tau_{T,s}} + f' n'_x n'_e - \frac{n'_{T,s}}{\tau_T^{sk}} + \frac{n_{T,s}}{\tau_T^{sk}} - \frac{n'_{T,s}}{\tau_T^{sk1}} + \frac{n_{T,t}}{\tau_T^{sk2}}, \quad (3)
\end{aligned}
$$

where $n_{T,t}$ and $n_{T,s}$ are the concentrations of intervalley X_t^- and intravalley X_s^-, respectively, and $\tau_{T,t}$ and $\tau_{T,s}$ stand for the corresponding recombination times. The rate $1/\tau_T^{sk2}$ refers to the transition from X_t^- of one valley to X_s^- of the other valley (i.e., intervalley transition from an intervalley excitonic state to an intravalley one), and $1/\tau_T^{sk1}$ represents the reverse process, cf. pink and orange arrows in Fig. 2(c). We emphasize that the transition of $1/\tau_T^{sk2}$ is more favorable than its reverse process $1/\tau_T^{sk1}$ [57], since X_t^- is higher in energy than X_s^-. And, all quantities in the K' valley are once again labeled by a superscript "$\prime$," to distinguish from those in the K valley.

We compute from Eqs. (1)–(3) the PL intensity for each individual excitonic channel via n/τ [58], where n and τ *generally* represent the excitonic concentrations and the corresponding recombination times appearing in the above equations. By directly solving the set of coupled rate equations, we obtain the time evolution of PL. In addition, by setting the left-hand side of the rate equations equal to zero, i.e., $dn/dt = 0$, we determine the laser power dependence of PL in steady state. The valley polarization η is associated with the distinction of PL intensity between the K and K' valleys, i.e., $\eta^i = [\mathrm{PL}^i(K) - \mathrm{PL}^i(K')]/[\mathrm{PL}^i(K) + \mathrm{PL}^i(K')]$ [59,60], with the superscript i standing for excitonic channels.

TABLE I. Relevant parameters [Eqs. (1)–(3)] used in our simulations [33,62–64]. The unit of time (τ) is in picoseconds, rates (β_0 and f) in $\mathrm{cm^2\ s^{-1}}$, power density (P_0) in $\mathrm{kW\ cm^{-2}}$, and electron density (n_e) in $10^{11}\ \mathrm{cm^{-2}}$.

$\tau_x = 500$	$\tau_T = 800$	$\tau_{xx} = 700$	$\tau_{T,s} = \tau_T$	$\tau_{T,t} = \tau_T$
$\tau_x^{sk} = 0.2\tau_x$	$\tau_{xx}^{sk} = 2\tau_x^{sk}$	$\tau_T^{sk} = 3\tau_x^{sk}$	$\tau_T^{sk2} = \tau_x^{sk}$	$\tau_T^{sk1} = 3\tau_x^{sk}$
$\beta_0 = 0.36$	$f = 0.1$	$P_0 = 10.2$	$n_e = 1.9$	

D. System and relevant parameters

We consider experimental PL measurements on monolayer WS_2 by Paradisanos *et al.* [22,61], in which the laser spot size is $l \sim 1\ \mu$m and the wavelength of generated photons is $\lambda = 532$ nm. This yields the exciton generation rate of $g \sim 5.35 \times 10^{20}\ \mathrm{s^{-1}\ cm^{-2}}$ for a laser power density of around 1 $\mathrm{kW\ cm^{-2}}$. Since the continuous wave (CW) laser was employed in the experiment, only the steady state, e.g., laser power dependence of PL spectrum, is measured. In addition to simulating the steady-state PL and comparing to experimental data, we go further beyond and consider a Gaussian pulse duration of $\sigma = 30$ ps to investigate the dynamics, i.e., $P \sim \exp[-4\ln(2)(t^2/\sigma^2)]$, with P the power density. An n-type monolayer WS_2 is considered, thus the generated trions are negatively charged. The remaining parameters adopted in our simulations [Eqs. (1)–(3)] are shown in Table I, unless otherwise stated. Below we discuss our simulated outcome about PL for the three cases mentioned above in the model, respectively.

III. RESULTS AND DISCUSSION

In this section we present our numerical outcome on valley dynamics of bright excitons introduced in Sec. II for cases (i)–(iii), respectively. Finally, we discuss the effect of dark exciton.

A. Valley dynamics of multiexcitonic states in a single valley

In this case we consider all excitonic states residing in the K valley (no intervalley scattering), referring to case I (see the model). Figure 1(a) shows the steady-state PL of excitons, trions, and biexcitons as a function of laser power. Clearly the PL intensity increases with the laser power, and our computed PLs for all excitonic channels are in very good agreement with the experimental data of Paradisanos *et al.* [22,65], cf. markers and solid curves. And the relative weight of PL, stemmed from different excitonic channels, strongly depends on the laser power. Remarkably, the biexciton channel, which has the weakest PL intensity at low laser powers, tends to prevail in PL over other excitonic states as the power strengthens. This is attributed to the quadratic dependence of biexciton population on exciton concentration, in contrast to that for trions having linear dependence [66] [Eq. (1)]. As a result, the PL intensity of biexcitons increases more dramatically with the power than that of trions, leading to the possible dominating behavior

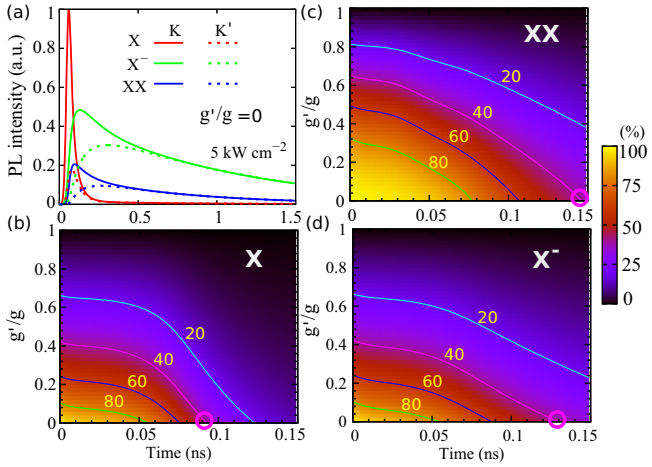

FIG. 3. (a) Time evolution of PL intensity in monolayer WS_2 for excitons (X), trions (X^-), and biexcitons (XX) in the K (solid curves) and K' (dotted curves) valleys, pumped by clockwise circularly polarized light, implying that optical excitation only takes place in the K valley. Valley polarization for X (b), XX (c), and X^- (d), as a function of time and the ratio of exciton generation rate (g'/g) between the K and K' valleys, with g (g') denoting the exciton generation rate in the K (K') valley. In (a), the PL intensity is normalized with respect to the exciton PL peak in the K valley. In (b)–(d), several values of contour lines of valley polarization are also shown. The pink circles mark the time that the valley polarization degree equals 40% at $g'/g = 0$. A Gaussian pulse duration of 30 ps is assumed.

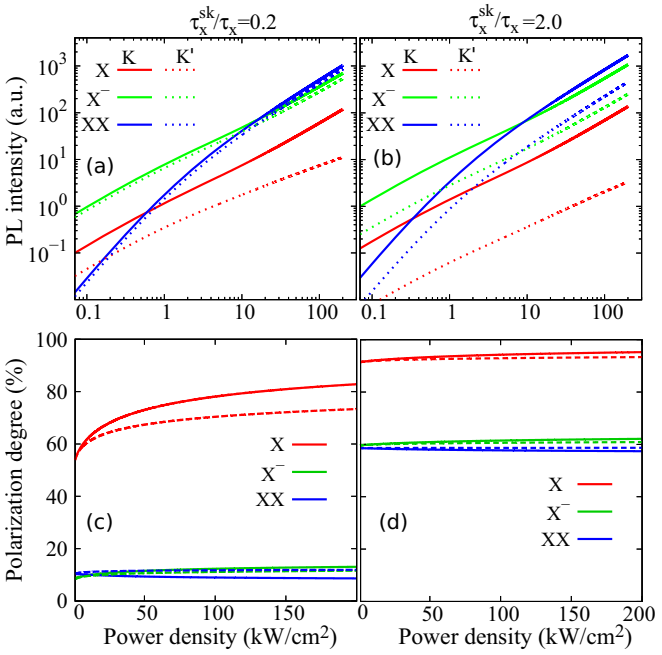

FIG. 4. (a) and (b) PL intensities of exciton (X), trions (X^-), and biexcitons (XX) in the K (solid curves) and K' (dotted curves) valleys of the monolayer WS_2 as functions of excitation laser power density. (c) and (d) Laser power density dependence of valley polarization, in which dashed curves represent valley polarization with a constant exciton-to-biexction transition rate β, i.e., $\beta = \beta_0$. (a) and (c) The relatively strong ($\tau_x^{sk}/\tau_x = 0.2$) intervalley scatterings, while (b) and (d) correspond to the relatively weak ($\tau_x^{sk}/\tau_x = 2.0$) ones. The pumping of clockwise circularly polarized incident lights is considered, implying that optical excitation only occurs in the K valley.

of the biexciton channel in PL spectra at high laser powers. Moreover, the dramatic increase of biexciton populations with laser power also implies that a power dependence of exciton-to-biexciton transition rate (β) may become essential, see the model. Neglecting the power dependence of β results in dotted lines in Fig. 1(a), which clearly shows inconsistence with the experimental data at high laser powers.

Note that the electron density in Fig. 1 is held fixed at $n_e = 1.9 \times 10^{11}$ cm^{-2} in our simulation. To verify the electron density dependence of valley dynamics, in Fig. S1 of the Supplemental Material (SM) [67], we show the PL at $n_e = 1.9 \times 10^{11}$, 1.0×10^{11}, and 0.5×10^{11} cm^{-2}, respectively. At low electron densities, the transition from exciton to trion is suppressed [Eqs. (1)–(3)], leading to relative enhancement of exciton PL and biexciton PL, cf. solid, dashed, and dotted curves in Fig. S1. In addition, since the trion concentration is associated with both n_e and n_x, the trion PL more sensitively depends on n_e at high laser power densities.

Now we turn to the dynamical picture. Figures 1(b) and 1(c) show the time evolution of PL at laser power densities equal to 0.5 and 5 kW cm^{-2}, respectively. The PL intensity in either case is normalized with respect to the corresponding PL peak of the exciton channel. Clearly the exciton PL intensity during the pulse duration of 30 ps increases rapidly. On the other hand, after the pulse duration, it decays more abruptly than that for trions and biexcitons, with the decay time far less than its recombination time $\tau_x \sim 500$ ps. This is attributed primarily to fast transitions from excitons to both biexcitons and trions, Eq. (1). By quenching the corresponding transitions [68], we find that the exciton PL decay time is considerably enhanced, see Figs. S2, S3, and S5(a) in the SM [67]. In addition, as the laser power is enhanced, the relative weight of PL intensity stemmed from the biexciton channel clearly rises, cf. Figs. 1(b) and 1(c), or Figs. S2(a) and S2(b) in the SM [67], similar to that in steady state. This is again because the biexciton population has a quadratic (more sensitive) dependence on the exciton density. We emphasize that similar dynamical features of PL spectra are obtained by increasing the pulse duration while keeping the laser power constant (not shown), since it is a combined effect of laser pulse duration and power density determining the generated exciton concentration.

B. Valley dynamics of intravalley excitonic states with intervalley scatterings

Now, let us switch on the intervalley scatterings, enabling transitions of excitonic states from one valley to the other, see case II of the model. We first consider the PL dynamics pumped by clockwise circularly polarized light fields, as shown in Fig. 3(a), for the PL evolution of excitons, trions, and biexcitons in the K and K' valleys. Since the valley selective transition rule depends on the helicity of light fields [9], the optical excitation only occurs in the K valley. It gives rise to an abrupt increase in the exciton PL intensity of the K valley during the excitation period. On the other hand, excitonic populations in the K' arise entirely from the

intervalley scatterings (charge transfer). Although the sum of PL intensity of the two valleys [60] for each individual excitonic channel may not amount to that in the single valley case (case I), which refers to $\tau_x^{sk} \to \infty$, $\tau_{xx}^{sk} \to \infty$, $\tau_T^{sk} \to \infty$ (vanishing intervalley scatterings), cf. solid and dotted curves of Fig. S3(b) in the SM [67], the intervalley scattering plays a minor role in the total PL of the two valleys in the parameter range considered here, as we will further emphasize later on in the steady state. Below, we turn to the valley polarization.

From Fig. 3(a) one can see a distinct imbalance of the PL intensity between the two valleys for all excitonic channels, characterizing the valley polarization of excitonic states. Figures 3(b)–3(d) show the valley polarization for excitons, biexcitons, and trions, respectively, mapping on time and the ratio of exciton generation rates (g'/g) between two valleys. As a result of the valley selective transition rule, the valley polarization of three excitonic channels all shrinks as the generation ratio increases from $g'/g = 0$ and identically vanishes at $g'/g = 1$. Therefore, g'/g offers a flexible tunability of valley polarizations. In addition, it is also found that the valley polarization for excitons decays much faster than that for biexcitons and trions, as indicated by the contour lines, cf. pink circles marking the valley polarization degree equal to 40% at $g'/g = 0$. Finally, the initial inertia of valley polarization with time shown in the contour lines, arises from a sustained generation of new excitonic states during the excitation period.

Now, we turn to the characteristics of steady states. To enhance the valley polarization, we consider clockwise circularly polarized light ($g'/g = 0$), implying that optical excitations only occurs in the K valley [9]. In Figs. 4(a) and 4(b) we show the PL intensity as a function of laser power for relatively strong ($\tau_x^{sk}/\tau_x = 0.2$) and weak ($\tau_x^{sk}/\tau_x = 2.0$) intervalley scatterings, respectively. In the former case, except for the X channel, the PL of the K and K' valleys is almost balanced, cf. solid and dotted curves, due to fast transfer of excitonic states from one valley to the other. In contrast, in the latter case, one can see a clear distinction of the PL intensity between the two valleys for all excitonic states, indicating an enhancement of valley polarization, cf. Fig. 4(c) for $\tau_x^{sk}/\tau_x = 0.2$ and Fig. 4(d) for $\tau_x^{sk}/\tau_x = 2.0$. In addition, we find that the valley polarization is almost immune to the laser power, especially for weak intervalley scatterings, consistent with experimental measurements of Plechinger *et al.* [52]. With strong intervalley couplings, the slight change of valley polarization when laser power increases, is mainly attributed to the dependence of exciton-to-biexciton transition rate β on the laser power. The valley polarization for constant $\beta = \beta_0$ is shown with dashed curves, from which one can see the power dependence is further suppressed.

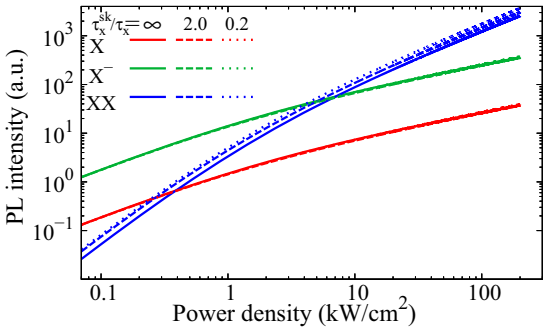

FIG. 5. PL intensity of exciton (X), trion (X^-), and biexciton (XX) in monolayer WS_2 as a function of power density, at $\tau_x^{sk}/\tau_x = \infty$, 2.0, and 0.2. The PL intensity at $\tau_x^{sk}/\tau_x = \infty$ is the same as that in the case of a single valley shown in Fig. 1(a), cf. Figs. 1(a) and 5.

Moreover, we emphasize that (i) the general behavior of PL spectra of the two valleys with the laser power is similar, e.g., the PL intensity of biexciton is the weakest at lower powers while it becomes predominant at higher ones and (ii) the PL intensity in the vanishing intervalley scattering limit will reduce to that of the single-valley case. For more systematic transitions of the PL and valley polarization in steady state from strong to weak intervalley scatterings, see Fig. S4 in the SM [67]. Although intervalley scatterings are crucial for valley depolarization, it is worth noting that the total PL intensity of the two valleys is almost immune to the intervalley scatterings, as shown in Fig. 5, implying the effect of intervalley scatterings on excitonic PL spectra may be negligible in the experiment of Ref. [22].

C. Valley dynamics of intra- and intervalley excitonic states with intervalley scatterings

After studying the valley dynamics of intravalley excitonic states, we are now ready to consider the case (case III of the model) involving both intra- and intervalley excitonic states in

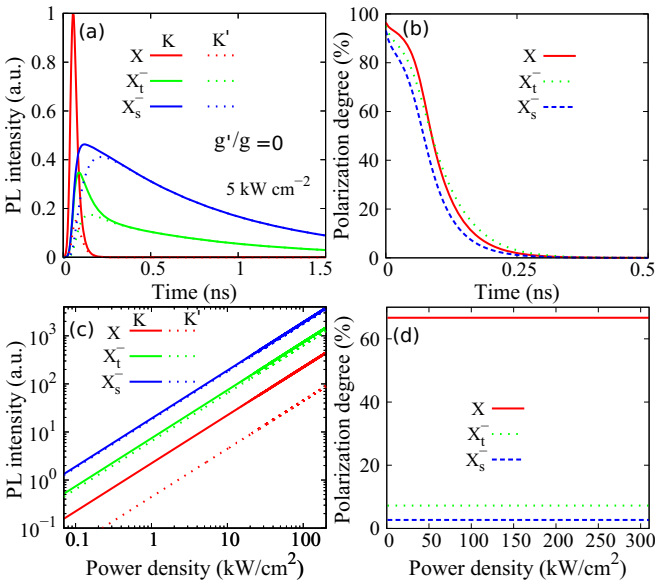

FIG. 6. (a) Dynamics of exciton (X), intervalley trion (spin triplet, X_t^-) and intravalley trion (spin singlet, X_s^-) PL intensity in the K (solid curves) and K' (dotted curves) valleys of monolayer WS_2. The PL intensity is normalized with respective to the exciton PL peak in the K valley. (b) Time evolution of valley polarization for X, X_t^-, and X_s^-. Dependence of (a) PL intensities in the K (solid curves) and K' (dotted curves) valleys, and (d) the corresponding valley polarizations, on the pumping laser power. The pumping of clockwise circularly polarized incident lights is assumed, implying that optical excitation only occurs in the K valley. In (a) and (b), a Gaussian pulse duration of 30 ps is considered.

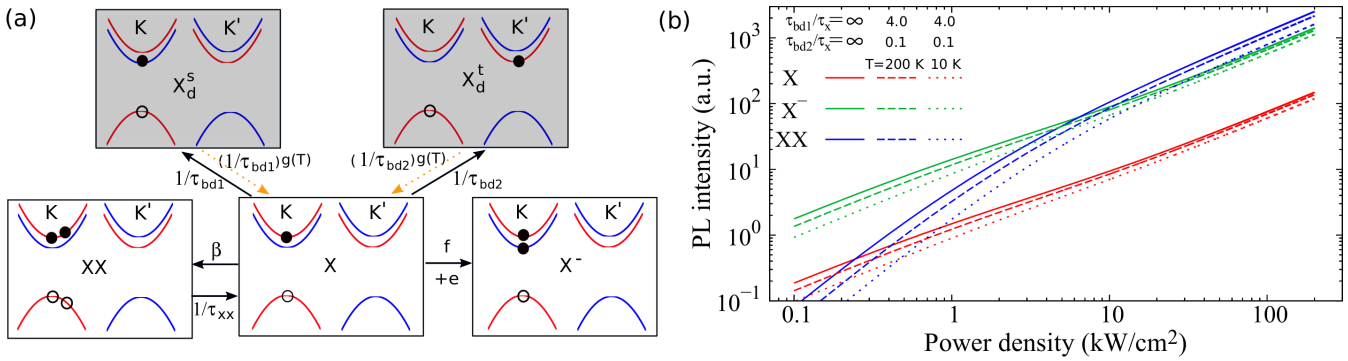

FIG. 7. Configurations of bright exciton (X), trion (X^-), biexciton (XX), intravalley spin-singlet dark exciton (X_d^s, spin forbidden), intervalley spin-triplet dark exciton (X_d^t, momentum forbidden) in monolayer WS_2. Red (blue) curves stand for spin-up (spin-down) states in the K and K' valleys. Filled (empty) black circles represent electrons (holes). The frames with white (gray) background correspond to bright (dark) excitonic states. The involved transition rates $1/\tau_{bd1}$, $(1/\tau_{bd1})g(T)$, $1/\tau_{bd2}$, and $(1/\tau_{bd2})g(T)$, are defined in Eq. (A1). (b) Total PL intensity of the K and K' valleys as a function of power density, at several values of τ_{bd1}/τ_x, τ_{bd2}/τ_x, and temperature T, with $\tau_{bd1}/\tau_x = \infty$, 4.0; $\tau_{bd2}/\tau_x = \infty$, 4.0; $T = 200$, 10 K.

the presence of intervalley scatterings. Here, for simplifying discussions, we exclude the biexciton channel and focus only on excitons and intravalley and intervalley trions, see the model.

In Fig. 6(a) we show the time evolution of PL for X, X_s^-, and X_t^- in both the K and K' valleys of monolayer WS_2. We consider once again the pumping of clockwise circularly polarized light fields, ensuring that optical excitation only takes place in the K valley. As a consequence, the PL of excitonic states in the K' valley arises entirely from intervalley scatterings. The distinction of excitonic PL intensities between the K and K' valleys underlies the valley polarization, the dynamics of which is shown in Fig. 6(b). We obtain the weakest valley polarization for the X_s^- channel, which is because (i) the population of excitonic states in the K valley dominates over that in the K' valley and (ii) the transition from X_t^- channel to X_s^- channel is more favorable than its reverse process, cf. pink and orange arrows in Fig. 2. Moreover, we find that the dynamics of valley polarization is almost immune to intravalley transition rates from excitons to trions (biexciton channel is excluded), cf. Fig. 6(b) and Fig. S5(b) (SM) [67], in contrast to the PL dynamics of the two valleys, cf. Fig. 6(a) and Fig. S5(a) (SM) [67].

Figures 6(c) and 6(d), respectively, show the steady-state PL and valley polarization dependence on the laser power, for X, X_t^-, and X_s^- in the K and K' valleys. The linear behavior of PL with the power density arises from the fact that we exclude the biexciton channel, which is associated with quadratic features in our model. And, the valley polarization for all excitonic channels remains essentially constant with the laser power, similar to that in case II.

D. The effect of dark excitons

In this section we discuss the effect of dark excitons on valley dynamics. Since intervalley scatterings are not essential for the total PL intensity of the system we consider (Sec. III B), we only focus on the excitonic states in a single K valley. In Fig. 7(a) we show the schematic of relevant scatterings taking place among bright excitonic states of exciton (X), trion (X^-), biexciton (XX), and dark states of spin-singlet dark exciton (X_d^s) and spin-triplet dark exciton (X_d^t). The corresponding rate equations are shown in Eq. (A1) (Appendix). For simplicity we have ignored the slow intervalley spin-flip scattering process between dark states X_d^s and X_d^t, which clearly does not affect the general feature of valley dynamics as the two dark states *interact* with the bright exciton in a similar way as shown in the figure.

The light emission, which characterizes total population of the bright excitons of the two valleys, depends on the competition between bright and dark states, where the latter may quench the light emission [37]. In Fig. 7(b) we show the total PL intensity of the two valleys as a function of laser power density, at $\tau_{bd1}/\tau_x = \infty$, $\tau_{bd2}/\tau_x = \infty$ (solid curves) referring to the case of no dark channels [cf. Fig. 1(a) and Fig. 7(b)], $\tau_{bd1}/\tau_x = 4.0$, $\tau_{bd2}/\tau_x = 0.1$, $T = 200$ K (dashed curves), and $\tau_{bd1}/\tau_x = 4.0$, $\tau_{bd2}/\tau_x = 0.1$, $T = 10$ K (dotted curves), respectively. Since the lowest energy transition is optically dark in WS_2, at a high temperature of $T = 200$ K adopted in the experiment of Ref. [22], the thermal energy could overcome the energy barrier $\Delta_{bd} \sim 30$ meV [55] and further suppress the effect of dark excitons to quench the light emission, cf. solid and dashed curves. Note that even at low temperatures, e.g. $T = 10$ K (dotted curves), the existence of dark excitons is expected to play a minor role when fit with the experimental data of a renormalized PL intensity, since the PLs for X, X^-, and XX *universally* becomes quenched by dark excitons. We should emphasize that here we only take into account the dark neutral excitons, a complex interplay among all dark excitonic channels including dark trions and dark biexcitons may generate new features of valley dynamics. More work is needed to investigate these possibilities.

IV. CONCLUDING REMARKS

We have developed a comprehensive model, which is composed of a complete set of rate equations, capturing both intra- and intervalley multichannel transitions of excitonic states including excitons, trions, and biexcitons. To systematically describe our model, we have considered three different cases, referring to three distinct experimental conditions. Then we have computed through our model the photoluminescence (PL)

spectra for each circumstance, both in dynamical (time evolution) and in steady-state (power dependence) frameworks. The PL tracks the information of valley populations, allowing us to further determine the valley polarization of all excitonic states. Our calculated PL is consistent with experimental data of Ref. [22], and we have found the relative weight of PL, originated from different excitonic channels, strongly depends on the laser power. On the other hand, the valley polarization remains essentially constant with the laser power, consistent with experimental measurements as well. In addition, it has been found that the intervalley scattering plays the vital role in the valley polarization. Moreover, for intervalley excitonic states, we have found that the spin-singlet intravalley X_s^- has the weakest valley polarization. As a final remark, monolayer WS_2 serves as a model system in our study here, but indeed, the same theory and similar discussions can be applied in other W-based TMDCs, and can even straightforwardly be extended to Mo-based TMDCs as well which have opposite ordering in energy regarding the two spin states of the conduction band [55], as compared to W-based TMDCs.

ACKNOWLEDGMENTS

This work was supported by CNPq, CAPES, FAPDF, and the Natural Science Foundation of China (Grant No. 11004120). We thank J. Cruz for enlightening input and fruitful discussions.

APPENDIX: RATE EQUATIONS IN THE PRESENCE OF DARK EXCITONS

The rate equations taking into account dark excitons of both spin-forbidden (X_d^s) and momentum-forbidden (X_d^t) types are written as [Fig. 7(a)]

$$\begin{aligned}
\frac{dn_x}{dt} &= g - \frac{n_x}{\tau_x} - f n_x n_e + \frac{n_{xx}}{\tau_{xx}} - 2\beta n_x^2 - \frac{n_x}{\tau_{bd1}} \\
&\quad - \frac{n_x}{\tau_{bd2}} + \frac{n_d^s}{\tau_{bd1}} g(T) + \frac{n_d^t}{\tau_{bd2}} g(T), \\
\frac{dn_T}{dt} &= -\frac{n_T}{\tau_T} + f n_x n_e, \\
\frac{dn_{xx}}{dt} &= -\frac{n_{xx}}{\tau_{xx}} + \beta n_x^2, \\
\frac{dn_d^s}{dt} &= -\frac{n_d^s}{\tau_x} + \frac{n_x}{\tau_{bd1}} - \frac{n_d^s}{\tau_{bd1}} g(T), \\
\frac{dn_d^t}{dt} &= -\frac{n_d^t}{\tau_x} + \frac{n_x}{\tau_{bd2}} - \frac{n_d^t}{\tau_{bd2}} g(T),
\end{aligned} \tag{A1}$$

in which n_x, n_T, n_{xx}, n_d^s, and n_d^t are the concentration of bright exciton (X), trion (X^-), biexciton (XX), spin-singlet dark exciton (X_d^s), and spin-triplet dark exciton (X_d^t) in the K valley, respectively; τ_x, τ_T, and τ_{xx} separately stand for the recombination times of exciton, trion, and biexciton; f represents the exciton-to-trion transition rate; n_e is the electron density in the K valley of an n-type monolayer TMDC; $1/\tau_{bd1}$ ($1/\tau_{bd2}$) denotes the transitions between X and X_d^s (X_d^t); and $g(T) = \exp(-\Delta_{bd}/k_bT)$ depends on temperature, with T the temperature, Δ_{bd} the energy difference between bright and dark excitons, and k_b the Bolzmann constant. Here we have assumed the dark states of X_d^s and X_d^t have the same energy, which is below the energy of the bright exciton by Δ_{bd}. Note that the scattering of $1/\tau_{bd1}$ involves spin flip, thus it is in general a slower process than the one corresponding to $1/\tau_{bd2}$ (no spin flip), see Fig. 7(a).

[1] F. C. Wu, F. Y. Qu, and A. H. MacDonald, Phys. Rev. B **91**, 075310 (2015).

[2] K. F. Mak, K. L. McGill, J. Park, and P. L. McEuen, Science **344**, 1489 (2014).

[3] G. B. Liu, D. Xiao, Y. G. Yao, X. D. Xu, and W. Yao, Chem. Soc. Rev. **44**, 2643 (2015).

[4] F. Y. Qu, A. C. Dias, J. Y. Fu, L. V. Lelovsky, and D. L. Azevedos, Sci. Rep. **7**, 41044 (2016).

[5] A. Splendiani, L. Sun, Y. B. Zhang, T. S. Li, J. Kim, C. Y. Chim, G. Galli, and F. Wang, Nano Lett. **10**, 1271 (2010).

[6] Q. H. Wang, K. Kalantar-Zadeh, A. Kis, J. N. Coleman, and M. S. Strano, Nat. Nanotechnol. **7**, 699 (2012).

[7] T. Cao, G. Wang, W. P. Han, H. Q. Ye, C. R. Zhu, J. R. Shi, Q. Niu, P. H. Tan, E. Wang, B. L. Liu, and J. Feng, Nat. Commun. **3**, 887 (2012).

[8] D. Oliveira, J. Fu, L. Villegas-Lelovsky, A. C. Dias, and F. Qu, Phys. Rev. B **93**, 205422 (2016).

[9] D. Xiao, G. B. Liu, W. X. Feng, X. D. Xu, and W. Yao, Phys. Rev. Lett. **108**, 196802 (2012).

[10] P. Dey, L. Y. Yang, C. Robert, G. Wang, B. Urbaszek, X. Marie, and S. A. Crooker, Phys. Rev. Lett. **119**, 137401 (2017).

[11] X. D. Xu, W. Yao, D. Xiao, and T. F. Heinz, Nat. Phys. **10**, 343 (2014).

[12] A. Srivastava, M. Sidler, A. V. Allain, D. S. Lembke, A. Kis, and A. Imamoğlu, Nat. Phys. **11**, 141 (2015).

[13] Y. Li, J. Ludwig, T. Low, A. Chernikov, X. Cui, G. Arefe, Y. D. Kim, A. M. van der Zande, A. Rigosi, H. M. Hill, S. H. Kim, J. Hone, Z. Li, D. Smirnov, and T. F. Heinz, Phys. Rev. Lett. **113**, 266804 (2014).

[14] K. F. Mak, K. L. He, J. Shan, and T. F. Heinz, Nat. Nanotechnol. **7**, 494 (2012).

[15] G. Aivazian, Z. R. Gong, A. M. Jones, R. L. Chu, J. Q. Yan, D. G. Mandrus, C. W. Zhang, D. Cobden, W. Yao, and X. D. Xu, Nat. Phys. **11**, 148 (2015).

[16] D. MacNeill, C. Heikes, K. F. Mak, Z. Anderson, A. Kormányos, V. Zólyomi, J. Park, and D. C. Ralph, Phys. Rev. Lett. **114**, 037401 (2015).

[17] G. Wang, X. Marie, B. L. Liu, T. Amand, C. Robert, F. Cadiz, P. Renucci, and B. Urbaszek, Phys. Rev. Lett. **117**, 187401 (2016).

[18] A. M. Jones, H. Y. Yu, N. J. Ghimire, S. F. Wu, G. Aivazian, J. S. Ross, B. Zhao, J. Q. Yan, D. G. Mandrus, D. Xiao, W. Yao, and X. D. Xu, Nat. Nanotechnol. **8**, 634 (2013).

[19] K. Hao, L. Xu, F. Wu, P. Nagler, K. Tran, X. Ma, C. Schüller, T. Korn, A. H. MacDonald, G. Moody, and X. Li, 2D Mater. **4**, 025105 (2017).

[20] K. Hao, G. Moody, F. Wu, C. K. Dass, L. Xu, C.-H. Chen, L. Sun, M.-Y. Li, L.-J. Li, A. H. MacDonald, and X. Li, Nat. Phys. **12**, 677 (2016).

[21] Z. L. Ye, D. Z. Sun, and T. F. Heinz, Nat. Phys. **13**, 26 (2017).

[22] I. Paradisanos, S. Germanis, N. T. Pelekanos, C. Fotakis, E. Kymakis, G. Kioseoglou, and E. Stratakis, Appl. Phys. Lett. **110**, 193102 (2017).

[23] S. Mouri, Y. Miyauchi, M. Toh, W. Zhao, G. Eda, and K. Matsuda, Phys. Rev. B **90**, 155449 (2014).

[24] A. C. Dias, J. Y. Fu, L. V. Lelovsky, and F. Y. Qu, J. Phys.: Condens. Matter **28**, 375803 (2016).

[25] J. S. Ross, F. S. Wu, H. Y. Yu, N. J. Ghimire, A. M. Jones, G. Aivazian, J. Q. Yan, D. G. Mandrus, D. Xiao, W. Yao, and X. D. Xu, Nat. Commun. **4**, 1474 (2012).

[26] Bound excitons could also exist especially at cryogenic temperatures.

[27] C. Robert, D. Lagarde, F. Cadiz, G. Wang, B. Lassagne, T. Amand, A. Balocchi, P. Renucci, S. Tongay, B. Urbaszek, and X. Marie, Phys. Rev. B **93**, 205423 (2016).

[28] M. Okada, Y. Miyauchi, K. Matsuda, T. Taniguchi, K. Watanabe, K. Shinohara, and R. Kitauralayak, Sci. Rep. **7**, 322 (2017).

[29] G. Plechinger, P. Nagler, A. Arora, R. Schmidt, A. Chernikov, A. G. del Águila, P. C. M. Christianen, R. Bratschitsch, C. Schüller, and T. Korn, Nat. Commun. **7**, 12715 (2016).

[30] H. Y. Yu, X. D. Cui, X. D. Xu, and W. Yao, Natl. Sci. Rev. **2**, 57 (2015).

[31] H. Yu, G.-B. Liu, P. Gong, X. Xu, and W. Yao, Nat. Commun. **5**, 3876 (2014).

[32] T. Yu and M. W. Wu, Phys. Rev. B **89**, 205303 (2014).

[33] M. Baranowski, A. Surrente, D. K. Maude, M. Ballottin, A. A. Mitioglu, P. C. M. Christianen, Y. C. Kung, D. Dumcenco, A. Kis, and P. Plochocka, 2D Mater. **4**, 025016 (2017).

[34] J. P. Echeverry, B. Urbaszek, T. Amand, X. Marie, and I. C. Gerber, Phys. Rev. B **93**, 121107(R) (2016).

[35] F. Volmer, S. Pissinger, M. Ersfeld, S. Kuhlen, C. Stampfer, and B. Beschoten, Phys. Rev. B **95**, 235408 (2017).

[36] G. B. Liu, W. Y. Shan, Y. G. Yao, W. Yao, and D. Xiao, Phys. Rev. B **88**, 085433 (2013).

[37] X.-X. Zhang, Y. You, S. Y. F. Zhao, and T. F. Heinz, Phys. Rev. Lett. **115**, 257403 (2015).

[38] M. R. Molas, C. Faugeras, A. O. Slobodeniuk, K. Nogajewski, M. Bartos, D. M. Basko, and M. Potemski, 2D Mater. **4**, 021003 (2017).

[39] X. X. Zhang, T. Cao, Z. G. Lu, Y. C. Lin, F. Zhang, Y. Wang, Z. Q. Li, J. C. Hone, J. A. Robinson, D. Smirnov, S. G. Louie, and T. F. Heinz, Nat. Nanotechnol. **12**, 883 (2017).

[40] M. Berghäuser, P. Steinleitner, P. Merkl, R. Huber, A. Knorr, and E. Malic, arXiv:1708.07725.

[41] E. Malic, M. Selig, M. Feierabend, S. Brem, D. Christiansen, F. Wendler, A. Knorr, and G. Berghaüser, Phys. Rev. Mater. **2**, 014002 (2018).

[42] A. M. Jones, H. Yu, J. R. Schaibley, J. Yan, D. G. Mandrus, T. Taniguchi, K. Watanabe, H. Dery, W. Yao, and X. Xu, Nat. Phys. **12**, 323 (2016).

[43] Y. You, X. X. Zhang, T. C. Berkelbach, and T. F. Heinz, Nat. Phys. **11**, 477 (2015).

[44] F. Gao, Y. J. Gong, M. Titze, R. Almeida, P. M. Ajayan, and H. B. Li, Phys. Rev. B **94**, 245413 (2016).

[45] C. Mai, Y. G. Semenov, A. Barrette, Y. Yu, Z. Jin, L. Cao, K. W. Kim, and K. Gundogdu, Phys. Rev. B **90**, 041414 (2014).

[46] C. R. Zhu, K. Zhang, M. Glazov, B. Urbaszek, T. Amand, Z. W. Ji, B. L. Liu, and X. Marie, Phys. Rev. B **90**, 161302 (2014).

[47] X. L. Song, S. Xie, K. Kang, J. Park, and V. Sih, Nano Lett. **16**, 5010 (2016).

[48] T. Godde, D. Schmidt, J. Schmutzler, M. Aßmann, J. Debus, F. Withers, E. M. Alexeev, O. Del Pozo-Zamudio, O. V. Skrypka, K. S. Novoselov, M. Bayer, and A. I. Tartakovskii, Phys. Rev. B **94**, 165301 (2016).

[49] In Ref. [33], the intervalley scattering is taken into account, but only excitons are considered.

[50] H. L. Zeng, J. F. Dai, W. Yao, D. Xiao, and X. D. Cui, Nat. Nanotechnol. **7**, 490 (2012).

[51] F. Rose, M. O. Goerbig, and F. Piéchon, Phys. Rev. B **88**, 125438 (2013).

[52] G. Plechinger, P. Nagler, J. Kraus, N. Paradiso, C. Strunk, C. Schüller, and K. Tobias, Phys. Status Solidi RRL **9**, 457 (2015).

[53] A. Singh, K. Tran, M. Kolarczik, J. Seifert, Y. Wang, K. Hao, D. Pleskot, N. M. Gabor, S. Helmrich, N. Owschimikow, U. Woggon, and X. Li, Phys. Rev. Lett. **117**, 257402 (2016).

[54] Z. Y. Zhu, Y. C. Cheng, and U. Schwingenschlögl, Phys. Rev. B **84**, 153402 (2011).

[55] K. Kośmider, J. W. González, and J. Fernández-Rossier, Phys. Rev. B **88**, 245436 (2013).

[56] T. F. Yan, X. F. Qiao, P. H. Tan, and X. H. Zhang, Sci. Rep. **5**, 15625 (2015).

[57] Here we treat $1/\tau_T^{sk1}$ and $1/\tau_T^{sk2}$ as two independent parameters. Note that one can in principle build up the relation between them through Boltzmann distribution.

[58] T. Schmidt, K. Lischka, and W. Zulehner, Phys. Rev. B **45**, 8989 (1992).

[59] P. K. Nayak, F. C. Lin, C. H. Yeh, J. S. Huang, and P. W. Chiu, Nanoscale **8**, 6035 (2016).

[60] Strictly speaking, it may be hard to *directly* distinguish PL spectra of the K and K' valleys. Here we emphasize the PL of each individual valley, as a result of it being proportional to the corresponding excitonic concentration.

[61] We have assumed that the transition rates are independent of temperature.

[62] L. Yuan and L. Huang, Nanoscale **7**, 7402 (2015).

[63] The transition rates β_0 and f in the two valleys are assumed the same.

[64] The same residual excess electron density is assumed in the K and K' valleys.

[65] This implies that the effect of intervalley scatterings on excitonic PL spectra may be negligible in the experiment of Ref. [22].

[66] A linear dependence of trion population on the exciton concentration does not necessarily mean its dependence on the laser power is also linear, since three coupled channels in equilibrium must be in a *balanced* state and the exciton density may not linearly depend on the power.

[67] See Supplemental Material at http://link.aps.org/supplemental/10.1103/PhysRevB.97.115425 for more details about PL intensity and valley polarization, which includes Refs. [60,9,7,68].

[68] One can also weaken f and β_0, to quench the transition from excitons to trions and biexcitons, see Eqs. (1)–(3) in the main text.